

Differential Cytostatic and Cytotoxic Action of Metalloporphyrins against Human Cancer Cells: Potential Platforms for Anticancer Drug Development

Punnajit Lim,[†] Atif Mahammed,[‡] Zoya Okun,[‡] Irena Saltsman,[‡] Zeev Gross,^{*,‡} Harry B. Gray,^{*,§} and John Termini^{*,†}

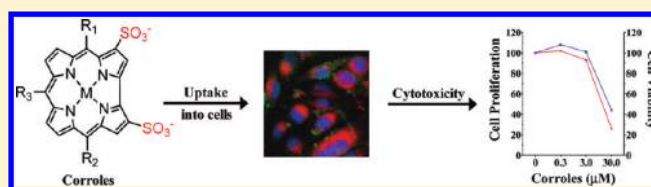
[†]Department of Molecular Medicine, Beckman Research Institute of the City of Hope, 1450 E. Duarte Road, Duarte, California 91010, United States

[‡]Schulich Faculty of Chemistry, Technion—Israel Institute of Technology, Haifa 32000, Israel

[§]Beckman Institute, California Institute of Technology, Pasadena, California 91125, United States

Supporting Information

ABSTRACT: A gallium(III)-substituted amphiphilic porphyrin noncovalently associated with a targeting protein was previously found by us to confer promising cytotoxic and antitumor activities against a breast cancer cell line and a mouse xenograft breast cancer model. To further explore potential anticancer applications, the cytostatic and cytotoxic properties of six nontargeted metalloporphyrins were evaluated against seven human cancer cell lines. Results indicated that toxicity toward human cancer cells depended on the metal ion as well as porphyrin functional group substitution. Ga(III)-substituted metalloporphyrin 1-Ga inhibited proliferation of breast (MDA-MB-231), melanoma (SK-MEL-28), and ovarian (OVCAR-3) cancer cells primarily by arrest of DNA replication, whereas 2-Mn displayed both cytostatic and cytotoxic properties. Confocal microscopy revealed extensive uptake of 1-Ga into the cytoplasm of melanoma and ovarian cancer cells, while prostate cancer cells (DU-145) displayed extensive nuclear localization. The localization of 1-Ga to the nucleus in DU-145 cells was exploited to achieve a 3-fold enhancement in the IC₅₀ of doxorubicin upon coadministration. Time-course studies showed that over 90% of melanoma cells incubated with 30 μM 1-Ga internalized metalloporphyrin after 15 min. Cellular uptake of 1-Ga and 1-Al was fastest and most efficient in melanoma, followed by prostate and ovarian cancer cells. Cell cycle analyses revealed that bis-sulfonated porphyrins containing Al(III), Ga(III), and Mn(III) induced late M phase arrest in several different cancer cell lines, a feature that could be developed for potential therapeutic benefit.



INTRODUCTION

Although cancer incidence is on the rise, mortality has slowly declined over the past few years due to improved understanding of tumor biology and more sophisticated diagnostic methods and therapeutic approaches.^{1,2} However, standard treatment regimens have not changed radically, and there is still an urgent need to develop better molecular platforms for improved cancer-targeting efficacy. Corroles, aryl-substituted corrin derivatives, are amenable to complex functionalization and can form stable chelates with a wide variety of metal ions, allowing for great flexibility in the design of molecules with unique physical and chemical properties.^{3,4}

Although corroles share limited structural features with the cobalt-chelating corrins present in vitamin B12, they display physical and chemical properties similar to porphyrins and chelate a diverse array of metal ions.^{5,6} Sulfonic acid substitution on β-pyrrole carbon atoms 2 and 17 or di- and tri-meso pyridinium substitution confers amphiphilic properties (Figure 1),^{7–9} which facilitates the formation of tight noncovalent complexes between metalloporphyrins and a variety of proteins such as human serum albumin (HSA),¹⁰ lipoproteins (LDL and HDL),¹¹ transferrin,¹² and a recombinant

adenovirus serotype 5 (Ad5) capsid penton base protein.¹³ This feature can be exploited to facilitate their transport into various cell types and allow for specific target design. Moreover, some metalloporphyrins, such as 1-Ga and 1-Al, are highly fluorescent, a property that can be used to monitor uptake and intracellular localization.¹⁴

Previous work demonstrated that 1-Ga noncovalently bound to a heregulin-modified protein directed at the human epidermal growth factor receptor (HER) was cytotoxic to breast cancer cells and induced tumor regression in a mouse xenograft model.^{13,14} To date, tumor-bearing animals treated with corroles have not shown any marked toxic side effects, suggesting their potential for anticancer drug development.^{11,14,15} These observations, along with renewed interest in exploring the potential therapeutic applications of porphyrins and related macromolecules,¹⁶ prompted our investigation of corroles as potential platforms for the development of chemotherapeutic agents. Because the efficiency of anticancer drugs can vary substantially among different cell types, we

Received: October 18, 2011

Published: December 20, 2011

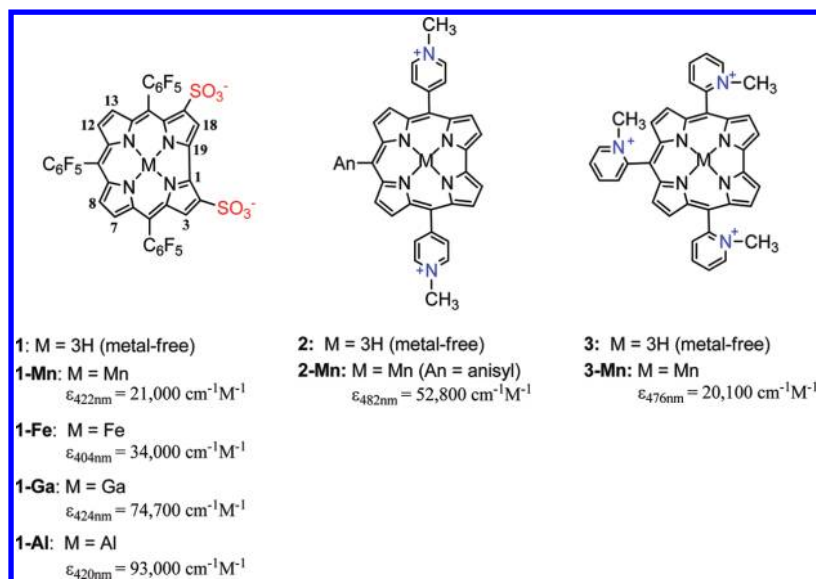


Figure 1. Structures and UV–vis spectroscopic data for metallocorroles used in this study.

decided to investigate whether the antiproliferative effects of corroles observed in breast cancer could be extended to other tumor-derived cell lines.

We examined the effects of a series of metallocorroles against seven NCI-60 cell lines¹⁷ derived from cancers of the breast, prostate, ovary, skin, lung, and colon (Table 1) and observed

Table 1. Human Cancer Cell Line Panel

cell line	tumor type	histology
HCT-116	colon	carcinoma
HCT-15	colon	adenocarcinoma
DU-145	prostate	carcinoma
NCI-H23	lung	adenocarcinoma
MDA-MB-231	breast	adenocarcinoma
SK-MEL-28	melanoma	malignant
OVCAR-3	ovarian	adenocarcinoma

differential cytotoxic and cytostatic responses with marked selectivity against melanoma, breast, and ovarian cancers. Kinetic studies of the intracellular uptake and accumulation of metallocorroles revealed cell-specific properties, which indicated their potential for tumor-selective targeting. Results are presented that show that the observed cytotoxic and cytostatic activities are dependent upon metal ion and functional group substitution and that corroles may also exert anticancer action by disrupting normal cell cycle progression.

EXPERIMENTAL PROCEDURES

Chemicals and Reagents. Bis-sulfonated and tris-pyridinium metallocorroles (Figure 1) were synthesized as previously described.^{5,6,18} The synthesis and characterization of 2-Mn was as follows: *p*-Anisaldehyde (49 μL , 0.4 mmol) was added to a 10 mL solution of pyridine-substituted dipyrromethane (178 mg, 0.8 mmol) in propionic acid, and the mixture was heated to reflux for 1 h. The residue obtained after solvent evaporation was washed with hot water, neutralized with ammonium hydroxide (25%), and washed again with hot water. Purification of corrole 2 was achieved by column chromatography (silica, CH_2Cl_2 followed by 1% methanol addition) affording pure 2 in 9% yield. Compound 2: $R_f = 0.34$ ($\text{CH}_2\text{Cl}_2/\text{EtOH}$ 10:1). UV/vis (CH_2Cl_2): λ_{max} ($\epsilon \cdot 10^{-3}$) = 420 (48.9), 574 (6.6), 623 (4.8), 649 (4.7). MS (MALDI-TOF): m/z (%): 558 (100) [M^+]. ¹H

NMR (400 MHz, C_6D_6): $\delta = 8.98$ (d, $J = 4.8$ Hz, 4 H), 8.80 (d, $J = 3.6$ Hz, 2 H), 8.69 (m, 4 H), 8.47 ppm (br. s, 4 H), 8.15 (d, $J = 8$ Hz, 2 H), $\delta = 8.02$ (d, $J = 4.8$ Hz, 4 H), 7.26 (d, $J = 8$ Hz, 2 H), 3.60 (s, 3 H). Manganese insertion and alkylation: 2-Mn was prepared by refluxing corrole 2 in pyridine with 15 equiv of $\text{Mn}(\text{OAc})_2 \cdot 4\text{H}_2\text{O}$ followed by chromatographic separation (silica, starting with CH_2Cl_2 and gradually adding methanol), affording 88% yield. The product was dissolved in hot THF, and an excess of methyl iodide was added to the solution, which was then left at 40 °C until complete precipitation. The solid material was collected by centrifugation and washed with THF and diethyl ether until the solvent was colorless affording pure 2-Mn in 94% yield. Compound 2-Mn: UV/vis (H_2O): λ_{max} ($\epsilon \cdot 10^{-3}$) = 354 nm (15.9), 492 nm (32.1), 601 nm (8.54), 684 nm (16.3). MS (MALDI-TOF LD⁺) m/z (%): 640 (20) [M^+], 625 (100) [$\text{M} - 15$]. These were dissolved in DMSO, and concentrations were determined by UV spectroscopy using the extinction coefficients listed in Figure 1. Stock solutions were further diluted in culture medium (RPMI 1640, Mediatech, Inc., Manassas, VA). The final amount of DMSO in drug solutions applied to tissue culture was <0.2%.

Reagents were obtained from the indicated suppliers: Hank's balanced salt solution (HBSS) without phenol red, Invitrogen Corp./Gibco, Carlsbad, CA; Triton X-100 and DAPI, Sigma-Aldrich, Inc., St. Louis, MO; Paraformaldehyde, Electron Microscopy Sciences, Hatfield, PA; Paclitaxel, Calbiochem, Gibbstown, NJ; Anti-Phospho-Histone H3 (Ser10) Antibody Alexa Fluor 647 Conjugate, Cell Signaling Technology, Danvers, MA; Hoechst 33342, Wheat Germ Agglutinin, Alexa Fluor 488 Conjugate, Invitrogen Corp./Molecular Probes, Carlsbad, CA; and Vectashield Hard-Set Mounting Medium with DAPI, Vector Laboratories, Burlingame, CA.

Human Cancer Cell Lines. Seven cell lines from the NCI-60 cell line panel representing six distinct tumor types (colon, prostate, lung, breast, melanoma, and ovarian) were used in this study (Table 1). Cells were grown in RPMI 1640 medium (Mediatech, Inc.) supplemented with 10% fetal bovine serum (Omega Scientific, Inc., Tarzana, CA), 100 U/mL penicillin, and 100 $\mu\text{g}/\text{mL}$ streptomycin (Life Technologies, Inc., Rockville, MD) and maintained at 37 °C under 5% CO_2 in a humidified incubator.

MTS and BrdU Assay. Cytotoxicity was determined by cell viability measurements using the CellTiter 96 Aqueous One Cell Proliferation Assay (MTS) from Promega (Madison, WI). Cytostatic activity was measured by the BrdU incorporation assay using the Cell Proliferation ELISA, BrdU (colorimetric assay) from Roche Applied Science (Indianapolis, IN). Cells were plated in seven 96-well dishes (5×10^3 cells per well; 0.1 mL per well) 24 h prior to treatment. Drug treatment was initiated by replacement with fresh media containing

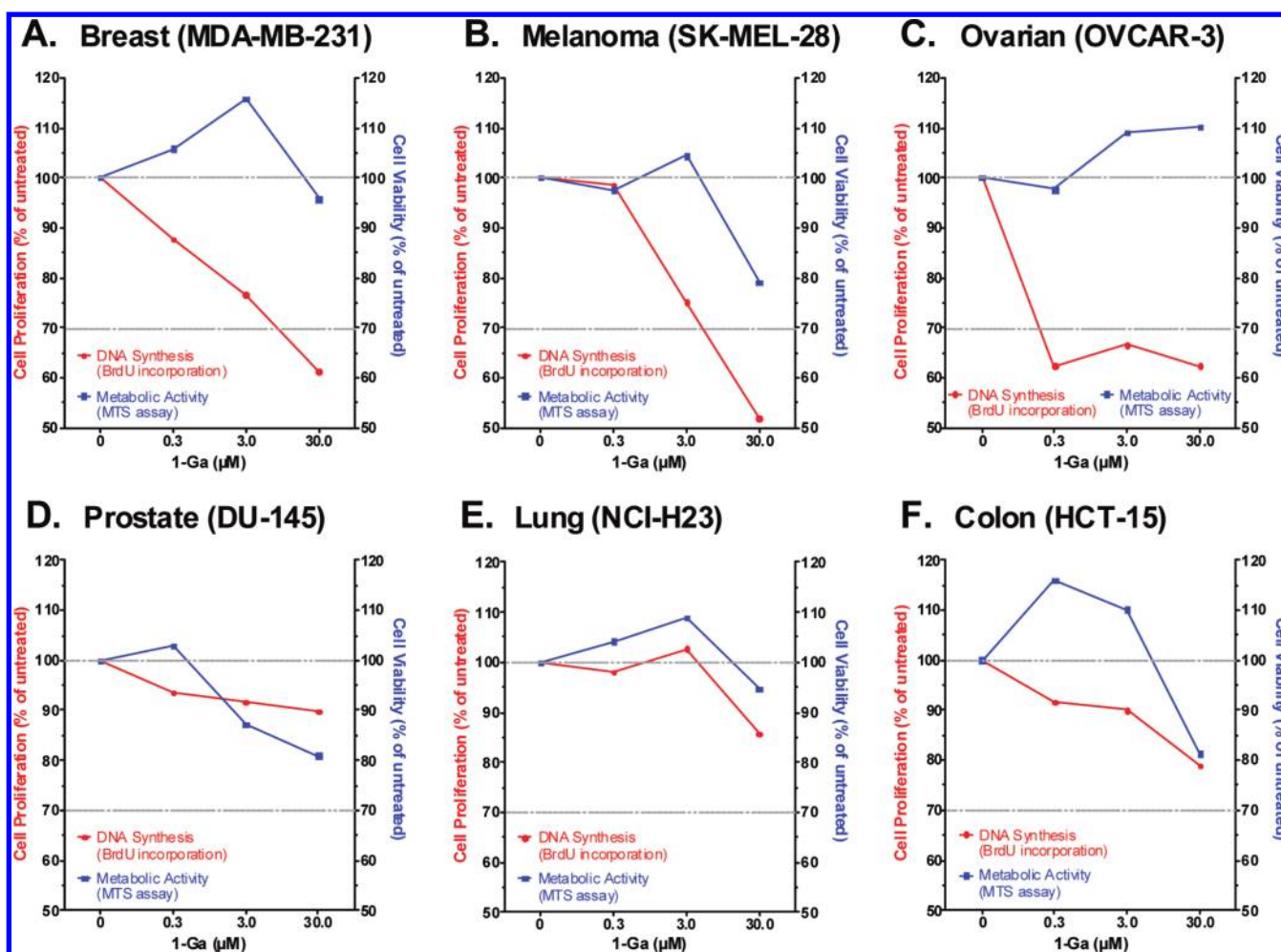


Figure 2. Cytotoxic and cytostatic activities of 1-Ga toward (A) MDA-MB-231 (breast), (B) SK-MEL-28 (melanoma), (C) OVCAR-3 (ovarian), (D) DU-145 (prostate), (E) NCI-H23 (lung), and (F) HCT-15 (colon) human cancer cells. Treated cells were incubated with 0.3, 3, or 30 μM 1-Ga, followed by determination of viability and DNA replication competency using the MTS and BrdU incorporation assays, respectively, as described in the Experimental Procedures.

0.3, 3, or 30 μM metallocorrole in 0.1 mL per well. All drug treatments were performed in the dark to minimize the effects of metallocorrole photochemistry. The MTS and BrdU assays were performed according to the manufacturers' directions once a day for six consecutive days. Absorbances were measured using a microplate reader (Synergy 4, Biotek Instruments, Inc., Winooski, VT) at 490 nm for MTS and 370 nm for BrdU. Experiments were performed in triplicate with standard deviation ranging from ~ 0.5 to 15% of the measured absorbances. The means from triplicate spectrophotometric data over a 7 day period were analyzed by nonlinear regression analysis using GraphPad Prism 5 (GraphPad Software, Inc., La Jolla, CA) to obtain a growth equation for each treatment. The first derivatives of nonlinear fits were used to obtain the rate of change, which was normalized to the control. The rate of cell proliferation (BrdU) or growth (MTS) of corrole-treated cells relative to control cells was reported as percent of untreated cells.

Confocal Microscopy. Confocal images of 1-Ga-treated cells were obtained using an upright LSM510 2-Photon microscope (Carl Zeiss MicroImaging, Inc., Thornwood, NY). Cells were seeded on glass coverslips at 1.5×10^5 cells per well, 2 mL per well in 24-well plates, and allowed to grow overnight. Compound 1-Ga was added directly to the cell media to 3 μM final concentration, followed by vortexing for 2 min at 500 rpm, and incubation for 3 h at 37 $^{\circ}\text{C}$, 5% CO_2 . The culture medium was aspirated, and cells were washed 2 \times with HBSS and then labeled with 5 $\mu\text{g}/\text{mL}$ WGA-Alexa Fluor 488 conjugate in HBSS for 10 min at 37 $^{\circ}\text{C}$. The labeling solution was removed; then, cells were washed 2 \times with PBS, fixed in 2% PFA/PBS for 20 min at room temperature (RT), followed by a final PBS wash. For mounting, the

coverslips containing cells were removed from 24-well dishes, dipped briefly in water, and directly mounted on slides containing 5 μL of Vectashield Hard-Set Mounting Medium with DAPI. Slides were placed at 4 $^{\circ}\text{C}$ in the dark for 12–24 h prior to imaging. Images were obtained at 40 \times magnification with constant fluorescence, exposure, and gain settings.

Point-Scanning Confocal Imaging of Uptake of Metallocorroles. The intracellular uptake of metallocorroles was quantified using the ImageXpress^{ultra} laser point-scanning confocal microscope (Molecular Devices, Inc., Sunnyvale, CA). A wavelength of 405 nm was used for excitation of DAPI and 1-Ga or 1-Al. DAPI fluorescence emission (blue) was measured with a 450 nm bandpass filter. Corrole fluorescence (red) was monitored using a 675 nm bandpass filter. Melanoma, prostate, and ovarian cancer cells were seeded in 96-well dishes (8×10^3 cells per well in 0.1 mL) and allowed to grow overnight. Compound 1-Ga or 1-Al was added directly to the media at 0, 0.3, 3.0, or 30 μM final concentration, vortexed for 2 min at 500 rpm, and incubated for 15 min or 1, 3, or 24 h at 37 $^{\circ}\text{C}$ under 5% CO_2 . Cells were then fixed and labeled in situ with WGA-Alexa Fluor 488 conjugate and DAPI to delineate the outer cell membrane and nuclear DNA, respectively. The quantification of DAPI fluorescence signals in each sample yielded the total number of cells in that population. The corresponding determination of red (1-Ga or 1-Al) fluorescence within each cells, corrected for background fluorescence from untreated cells, established the number of cells containing metallocorroles. For each corrole concentration at various time points, fluorescence data were obtained for 5500–7000 individual cells. Data

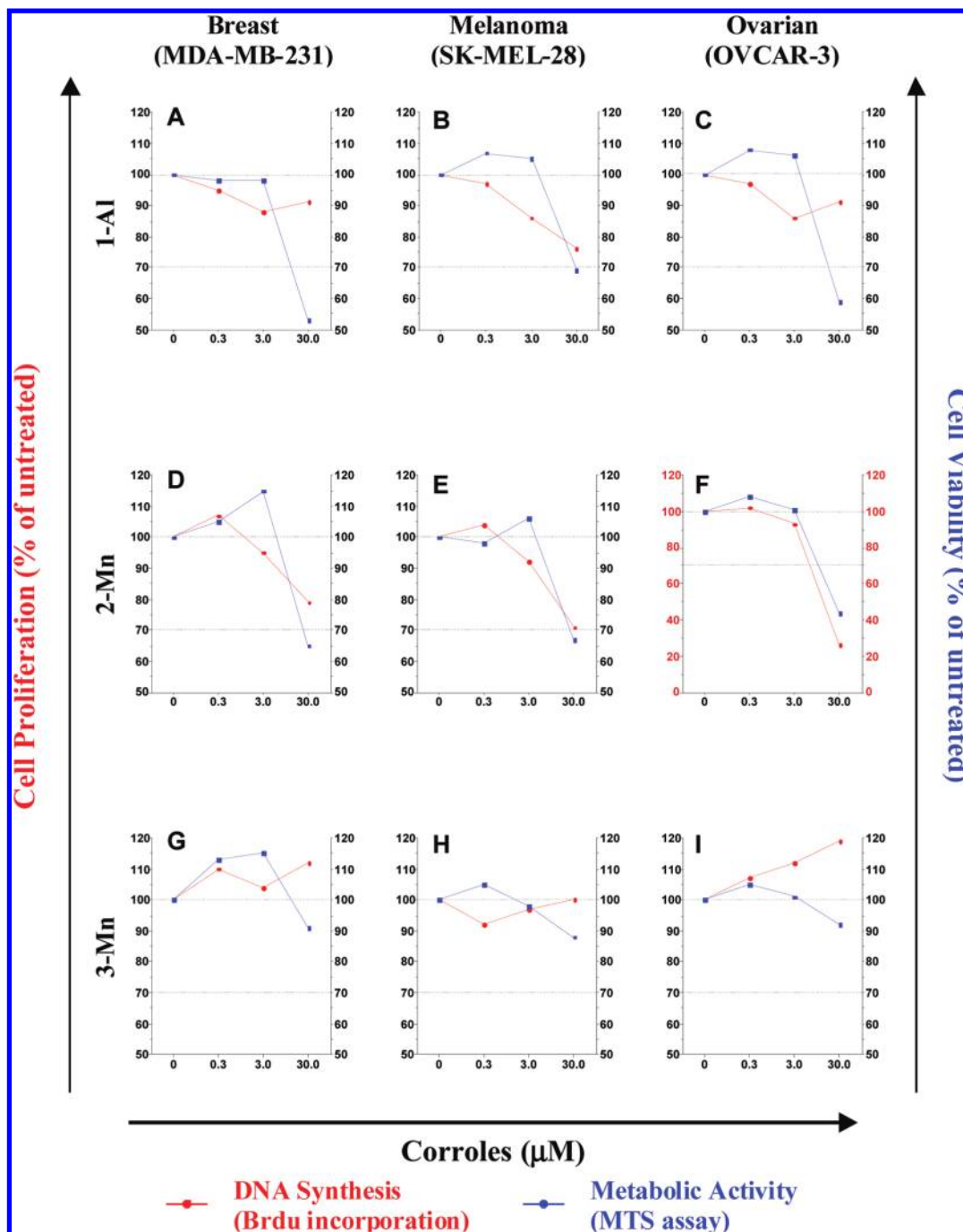


Figure 3. Cytotoxic and cytostatic activities of Al(III)- and Mn(III)-substituted corroles against MDA-MB-231 (breast), SK-MEL-28 (melanoma), and OVCAR-3 (ovarian) cancer cells. Cells were treated with 0.3, 3, and 30 μM 1-Al (A–C), 2-Mn (D–F), or 3-Mn (G–I).

were acquired on the ImageXpress^{ultra} at 81 sites in each well using a 20x Plan Fluor objective equipped with DAPI and Cy5 filter cubes. Image and statistical analyses were performed using the MetaXpress and AcuityXpress image analysis software, respectively. The number of cells containing metallocorroles relative to total number of cells was reported as percent of corrole-positive cells; the median fluorescence intensity was calculated for each treatment and represented in a 3-axis graph using Origin 7.0 (OriginLab Corp., Northampton, MA).

Cell Cycle Analysis. Metallocorrole-induced perturbations of the cell cycle were examined using ImageXpress^{ultra} in conjunction with the cell cycle application module for the MetaXpress image analysis software. Statistical analyses were performed using AcuityXpress cellular informatics software. Cells were plated in 96-well dishes (8×10^3 cells per well in 0.1 mL) and allowed to grow overnight.

Metallocorroles (30 μM final concentration of 1-Ga, 1-Fe, 1-Mn, 1-Al, 2-Mn, or 3-Mn) or paclitaxel (0.1 μM) was added to cell-containing media. After 24 h at 37 °C under 5% CO_2 , cells were washed 2 \times with PBS and fixed in 2% PFA/PBS for 20 min at RT, followed by three additional PBS washes of 5 min each. Immunostaining was carried out according to the manufacturer's protocol. Briefly, cells were incubated in blocking buffer (0.3% Triton X-100/PBS) for 1 h at RT. Anti-Phospho-Histone H3 (Ser10) Antibody (Alexa Fluor 647 Conjugate) was diluted at 1:400 ratio in antibody dilution buffer (1% BSA/0.3% Triton X-100/PBS) and applied to cells after the removal of blocking buffer. Cells were incubated at 4 °C overnight in the dark. After they were washed with PBS (3 \times) to remove free antibody, cells were incubated for 30 min with Hoechst Dye (3 $\mu\text{g}/\text{mL}$ in PBS), then rinsed once, and stored in PBS at 4 °C for imaging. Images were

acquired on the ImageXpress^{ultra} at 16 sites in each well as described above. For each treatment, fluorescence data and cell cycle determination were obtained for ~2000 individual cells. The number of cells in various phases of the cell cycle relative to the total number of cells was reported as percent cells in respective phases of the cell cycle.

1-Ga as a Chemotherapy Adjuvant. The potential application of metallocorroles as a carrier molecule for chemotherapeutic agents was investigated by a coadministration of 1-Ga with doxorubicin. Cells were plated in 96-well dishes (5×10^3 cells per well in 0.1 mL) and allowed to grow overnight. Doxorubicin alone (final concentrations of 0.01, 0.1, 0.5, 1.0, or 1.75 μM) or in combination with 3 μM 1-Ga was added to cell-containing media. Following 48 h of exposure at 37 °C, cell viability was determined using the MTS assay according to the manufacturer's instructions. Absorbances were measured using a microplate reader (Synergy 4, Biotek Instruments, Inc.) at 490 nm. Experiments were performed in triplicate with standard deviations ranging from ± 0.02 to ± 0.12 . Spectrophotometric data were analyzed by sigmoid dose-response, nonlinear regression analysis, and the IC₅₀ values were calculated using GraphPad Prism 5 (GraphPad Software, Inc.).

RESULTS AND DISCUSSION

Differential Toxicity of 1-Ga toward Human Cancer Cells. In light of promising results obtained against breast cancer models, the activity of 1-Ga (Figure 1) toward seven human cancer cell lines representing six distinct tumor types (Table 1) was initially examined. Each cell line was incubated in complete (i.e., serum-containing) medium with 1-Ga at 37 °C for up to 7 days. The effects of 1-Ga against cancer cell lines were evaluated every 24 h for up to 6 days using the MTS and BrdU assays, which measure cytotoxic and cytostatic activities, respectively. The integrated values for cytotoxicity (MTS assay) and proliferative capacity (BrdU incorporation) as a function of 1-Ga concentration are shown in Figure 2. The two colon cancer cell lines, HCT-116 and HCT-15, exhibited nearly identical responses to 1-Ga; thus, data for only HCT-15 are shown (Figure 2F). In all lines, cell killing (cytotoxicity) by 1-Ga was only evident at relatively high concentrations (30 μM). In contrast, inhibition of DNA replication by 1-Ga (cytostatic activity) was observed at concentrations as low as 300 nM in breast and ovarian cancer cells (Figure 2A,C) and 3 μM in melanoma cells (Figure 2B). Approximately 40–50% inhibition of cell proliferation was observed in all three cell lines at 30 μM 1-Ga. In contrast, the cytostatic and cytotoxic effects of 1-Ga against prostate, lung, and colon cancer cells were found to be negligible, suggesting defined rather than broad toxicological activity (Figure 2D–F).

Cytotoxic and Cytostatic Activities of Differentially Substituted Metallocorroles. The toxicological properties of metallocorroles toward cancer cell lines were influenced by both the chelated metal ion and the corrole functional group substitution pattern. Metal ion effects on the cytotoxic and cytostatic activities within a corrole series were examined by substituting Al(III) for Ga(III) in bis-sulfonated corrole 1. Compound 1-Al showed significantly greater cytotoxicity in the MTS assay as compared to 1-Ga against breast and ovarian carcinoma lines at the 30 μM dose (Figure 3A,C vs Figure 2A,C), although there was little change in cytotoxicity toward melanoma cells as a result of Al(III) substitution. Significant dose-dependent cytostatic activity for 1-Al was only observed against melanoma cells (Figure 3B). Cationic Mn(III) substituted meso-bis *para*-pyridinium and tris *ortho*-pyridinium corroles (2-Mn and 3-Mn, respectively, Figure 1) were also studied for activity against melanoma, breast, and ovarian

cancer cell lines. The bis-pyridinium 2-Mn demonstrated cytostatic and cytotoxic activities against all three cell lines (Figure 3D–F). The activity was most pronounced against the ovarian cancer cell line (Figure 3F). Approximately 60% of OVCAR-3 cells were killed at a dose of 30 μM , whereas 80% of the surviving fraction exhibited DNA replication arrest. In contrast, tris-pyridinium 3-Mn showed neither cytostatic or cytotoxic activity at all concentrations tested (Figure 3G–I). Ga(III) and Al(III) derivatives of 2 and 3 were also prepared but did not display any unusual biological or physicochemical properties to warrant further testing. Compounds 2-Fe and 3-Fe compounds were synthesized but were found to be unstable and were not considered further.

Metallocorrole metal ion and functional group substitution will influence their association with potential carrier proteins, cell membranes, DNA, and other potential molecular targets as well as their redox properties. For example, anionic bis-sulfonated metallocorroles with structure 1 have been shown to interact strongly with lipoproteins, while cationic dipyrrolyl analogues 2 were predominantly unbound or only weakly associated with serum proteins.¹⁹ Thus, cellular uptake of 2-Mn may not be dependent on protein carriers. The *para*-pyridinium substitution of 2-Mn, coupled with its hydrophobic tetrapyrrole core, stabilizes interactions with DNA via electrostatic binding to the phosphate backbone and intercalation, respectively, in a manner analogous to ethidium bromide, whereas *ortho*-pyridinium-substituted 3-Mn cannot intercalate into DNA.⁷ This may explain the significant inhibition of DNA synthesis and subsequent cytotoxicity observed for 2-Mn across three different cancer cell lines, whereas 3-Mn was completely inactive against all tested lines (Figure 3).

The redox chemistry of Mn(III)-substituted corroles toward reactive oxygen and nitrogen species may also contribute to their biological activity. Mn(III)-substituted corroles are pro-oxidants and have been shown to initiate lipid peroxidation as well as catalyze the oxidation of aromatic thiols to sulfoxides via the intermediacy of high-valent Mn(V)oxo complexes.^{6,11} The absence of redox chemistry for Ga(III) and Al(III) would suggest that the toxicity against cancer cell lines observed for 1-Ga and 1-Al must be independent of free-radical mechanisms. However, 1-Ga and 1-Al may induce oxidative damage indirectly. For example, it has been shown that gallium compounds can enhance the cellular uptake of iron from transferrin,²⁰ which could increase the potential for oxidative damage via Fenton type reactions.²¹ Gallium complexes are also known inhibitors of ribonucleotide reductase, presumably because they can compete with iron binding at the active site.^{22,23} This would reduce dNTP levels in the nucleotide precursor pool and restrict *de novo* DNA synthesis, which could account in part for the cytostatic activities observed for 1-Ga and 1-Al.

There has been longstanding interest in the use of Ga(III) compounds for cancer treatment;²⁴ however, drug development has been hampered by the availability of suitable ligands that can stabilize Ga(III) compounds against hydrolysis and facilitate cell permeability.²³ Nitrate and chloride gallium salts have been extensively investigated for therapeutic purposes and have been evaluated in phase I/II clinical trials against hepatoma, lymphoma, and bladder cancer.^{24–26} The cytostatic effects of GaNO₃ against lymphoma cells in culture have been reported to occur around 120 μM , while cytotoxicity becomes apparent at ~500 μM .^{25,27} Chelated Ga(III) derivatives appear to have improved biological activity relative to the free salts,

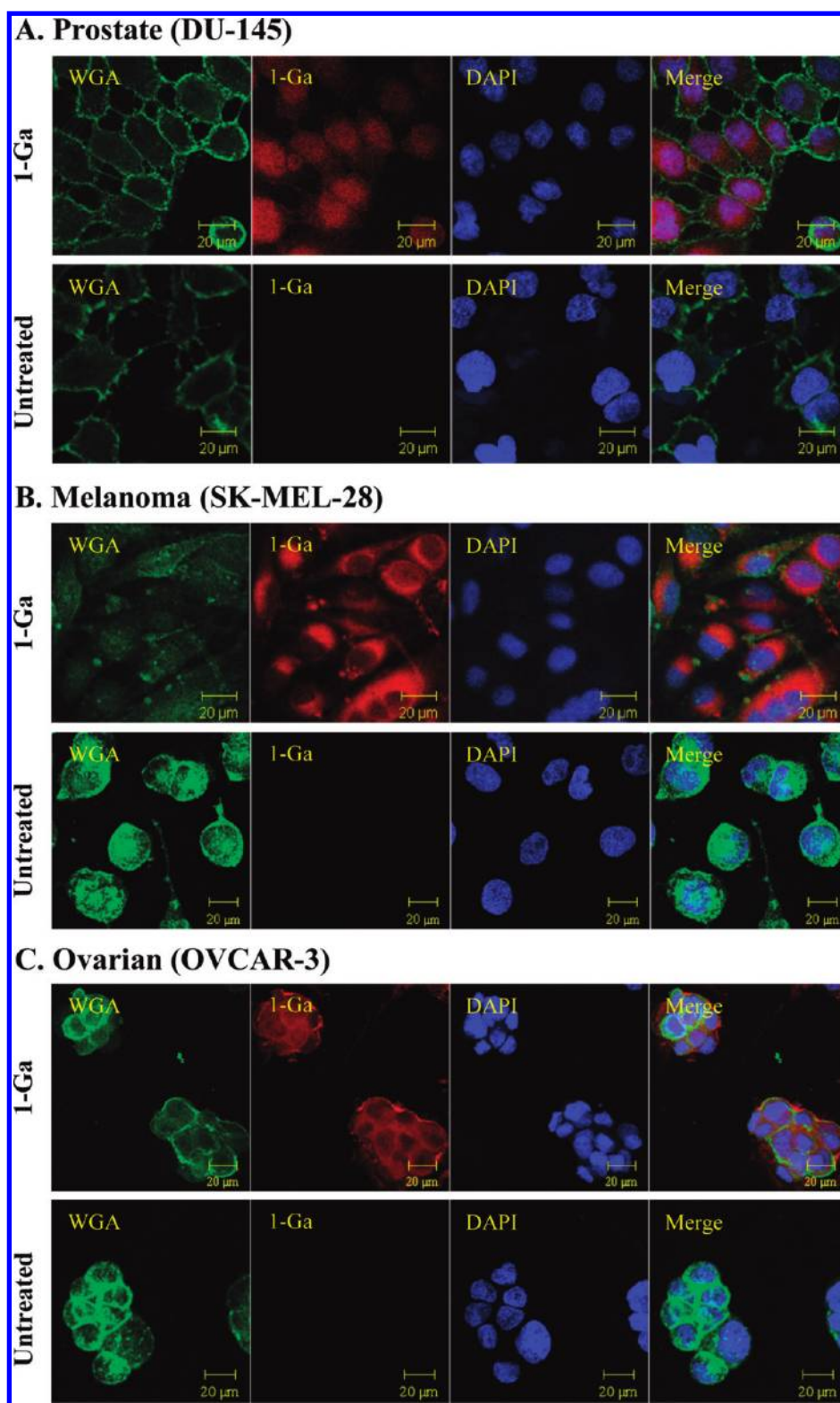


Figure 4. Intracellular accumulation of 1-Ga (red fluorescence). (A) DU-145 (prostate), (B) SK-MEL-28 (melanoma), and (C) OVCAR-3 (ovarian) cells were treated with 1-Ga ($3 \mu\text{M}$ for 3 h) or untreated (medium only). Cells were stained with Alexa Fluor 488 conjugated to WGA and DAPI. Images were obtained at 40 \times magnification using an upright confocal microscope and displayed in three-color channels with a merged image. Fluorescence settings were kept constant between imaging, and images were captured at fixed exposure and gain settings. The scale bar represents 20 μm .

and gallium maltolate was described as exerting cytotoxicity against the CCRF-CEM leukemic cells at $\sim 65 \mu\text{M}$ ²⁷ and between 25 and 35 μM against several hepatoma lines.²⁸ These latter values are similar to what we observed for Ga(III)

corroles (Figure 2). In our hands, 1-Ga was most effective as a cytostatic agent, inhibiting DNA replication in 40% of OVCAR-3 cells at a dose of 0.3 μM . To the best of our knowledge, this is the first report of a Ga(III) compound displaying appreciable

submicromolar cytostatic activity. The enhanced chelate stability relative to the maltolate derivative, and particularly in view of the efficient cellular uptake revealed in these studies (see below), suggest that corroles may represent an improved platform for therapeutic metal ion delivery to cancer cells.

Uptake and Localization of 1-Ga. To assess whether the variability in cytostatic activity of 1-Ga against melanoma and ovarian relative to prostate cancer cells resulted from differences in uptake and/or intracellular localization, confocal image analyses were performed. Cells were incubated with 3 μM 1-Ga in complete media for 3 h or in media alone (Figure 4A–C). Cells were labeled with DAPI and WGA-Alexa Fluor 488 conjugate to image nuclear DNA (blue fluorescence) and *N*-acetylglucosamine of the plasma membrane (green fluorescence), respectively. Compound 1-Ga was readily observable due to its intense red fluorescence a feature absent in untreated cells (Figure 4). In the prostate DU-145 cells (Figure 4A), the colocalization of blue and red fluorescence observed in the merged images indicated nuclear localization of 1-Ga. In contrast, melanoma and ovarian cancer cells retained strong blue nuclear fluorescence from DAPI in the presence of 1-Ga and exhibited mainly cytoplasmic accumulation of metallo-corrole in the merged images (Figure 4B,C).

The cell-specific mechanisms of metallocorrole uptake in these cancer lines are presently under investigation; however, it is likely that internalization of bis-sulfonated corroles of structure 1 was facilitated through noncovalent association with serum carrier proteins.¹³ The binding of metallocorroles 1-Ga, 1-Fe, and 1-Mn to lipoproteins, LDL, HDL, and transferrin has been previously described.^{11,19} Structurally related porphyrins have been shown to bind to the LDL receptor as well as the mitochondrial outer membrane-associated benzodiazepine receptor.^{29,30} More recently, porphyrins have been shown to enter the mitochondria via the ABCB6 transporter of the ATP binding cassette superfamily.³¹ Analogous mechanisms may be involved in the uptake and subcellular accumulation of metallocorroles. The molecular basis for the nuclear localization of 1-Ga in the DU-145 prostate line is unclear; however, it is possible that this metallocorrole is not retained strongly within lysosomes once internalized in these cells and can more readily enter the nucleus in a manner that may be dependent on protein carriers. It is interesting that the nuclear accumulation of 1-Ga in DU-145 cells (Figure 4A) did not adversely affect growth or replication within the sensitivity limits of our assays.

Time-Dependent Uptake of 1-Ga and 1-Al. The ImageXpress^{ultra} system, a laser point-scanning confocal microscope that integrates digital microscopy and flow cytometry, was used to measure the time course of uptake of metallocorroles and the degree of intracellular accumulation. Uptake was studied only for 1-Ga and 1-Al since Mn(III)-substituted corroles are not fluorescent. Time-dependent accumulation at a 3.0 μM dose was measured in melanoma, ovarian, and prostate cancer cells, and results are presented in Figure 5A,B for 1-Ga and 1-Al, respectively. The *y*-axis indicates the percentage of cells displaying detectable corrole fluorescence, whereas the *z*-axis shows the median fluorescence intensity, which is directly proportional to the extent of corrole uptake. In general, the internalization of 1-Al was more efficient than 1-Ga. For example, after 15 min, ~80% of melanoma cells displayed 1-Al fluorescence (Figure 5B), whereas <20% of cells were labeled using 1-Ga at the same time point (Figure 5A). Approximately 85% of the DU-145 prostate cells display 1-Al fluorescence after 3 h, whereas <40% are labeled with 1-Ga at this time interval.

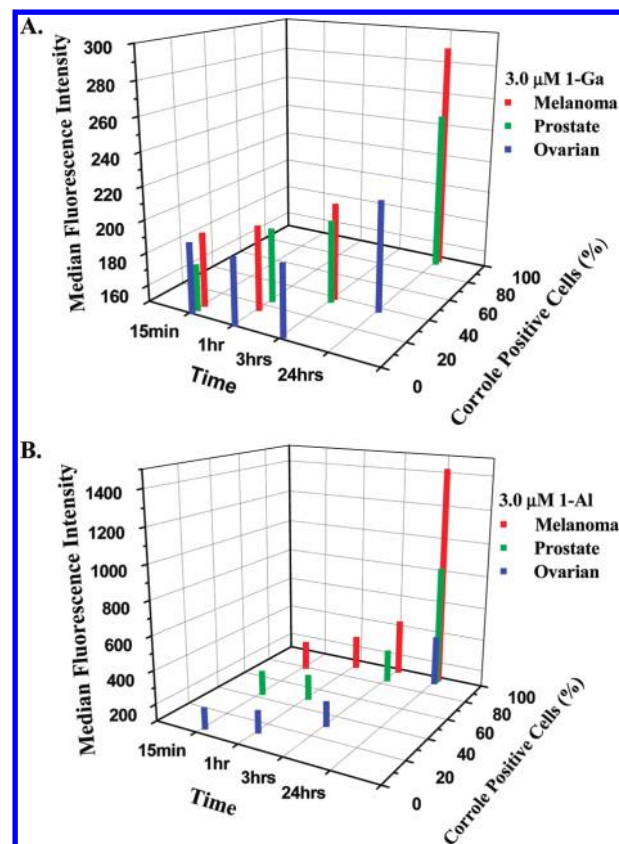


Figure 5. Time-dependent uptake and accumulation of 1-Ga and 1-Al by SK-MEL-28 (red), DU-145 (green), and OVCAR-3 (blue) cancer cells determined using the ImageXpress^{ultra} system. Cells were exposed to 3.0 μM 1-Ga (A) or 1-Al (B) for the time points indicated on the *x*-axis. The presence of metallocorrole within cells yielded red fluorescence, presented as a percentage of corrole positive cells (*y*-axis). The extent of corrole uptake was directly proportional to the median fluorescence intensity (*z*-axis). Cell images were obtained at 20 \times magnification using filters for blue (DAPI) and red fluorescence.

After 24 h, 100% of cells from all three cancer lines displayed 1-Al fluorescence, whereas quantitative labeling was only observed for melanoma and prostate lines with 1-Ga. The uptake of 1-Ga was very slow in ovarian cancer cells; after 24 h of incubation, only ~40% of cells exhibited fluorescence. Melanoma cells displayed the most rapid and efficient uptake with either metallocorrole, followed by prostate and ovarian cancer cells. The efficient uptake into SK-MEL-28 melanoma cells is consistent with transferrin-mediated transport of metallocorroles,¹² since these cells are well-known to avidly accumulate iron via this mechanism.³² The efficiency of 1-Ga uptake did not necessarily correlate with biological activity. For example, prostate cancer cells demonstrated efficient uptake as well as nuclear localization; yet, DNA replication was only inhibited in ~10% of the cell population at 30.0 μM (Figure 2D). Toxicity at this dose was only ~20%. Although the uptake of 1-Ga was least efficient in the ovarian carcinoma line, a therapeutically relevant dose of 300 nM was sufficient to elicit significant (~40%) arrest of DNA synthesis (Figure 2C).

Metallocorroles Induce Mitotic Arrest. To further investigate potential mechanisms of metallocorrole-induced cytostatic and cytotoxic action, cell cycle analyses were performed using the ImageXpress^{ultra}. Melanoma, ovarian, and breast cancer cells were treated with 30 μM 1-Ga, 1-Al, 1-Fe, 1-Mn, 2-Mn, and 3-Mn. As a control, cells were also

treated with 0.1 μM paclitaxel, which blocks cell division at the G2/M checkpoint. Classification of cell cycle phases was based on the fluorescence intensity of DNA dye (Hoechst 33342) and mitotic-specific stains anti-Phospho-Histone H3 (Ser10) Alexa fluor 647 conjugate. Cells progressing from G0/G1 to G2/M double their DNA content and can be identified by the corresponding increase in Hoechst 33342 fluorescence intensity. Changes in fluorescence intensity induced by phosphorylation at Ser10 of histone H3, a modification tightly correlated with chromosome condensation during mitosis, were used to detect cells in M phase. A representative cell cycle data set is shown in Figure 6 for melanoma cells following exposure

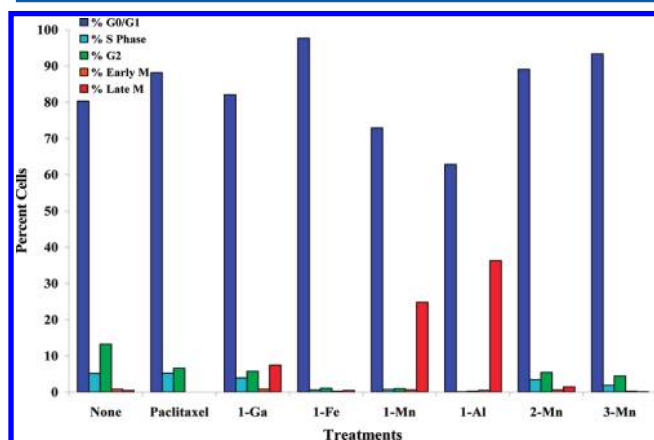


Figure 6. Influence of metalloporphyrins on cell cycle progression of SK-MEL-28 cells. Cells were incubated with various metalloporphyrins (30 μM 1-Ga, 1-Fe, 1-Mn, 1-Al, 2-Mn, and 3-Mn), paclitaxel (0.1 μM), or complete medium alone. Quantitation of the distribution of cell cycle phases was based on the fluorescent intensity of Hoechst 33342 and Anti-Phospho-Histone H3 (Ser10) Antibody (Alexa Fluor 647 Conjugate) at 10 \times magnification using the ImageXpress^{ultra} system.

to various metalloporphyrins. For untreated cells, the majority (~80%) were observed to be in G0/G1 followed by G2, S, and M. Inhibition of tubulin assembly by paclitaxel inhibited mitosis and blocked cells at the G2/M checkpoint. Metalloporphyrins that did not exhibit cytostatic or cytotoxic activity such as 3-Mn (Figure 3G–I) and 1-Fe (data not shown) displayed cell cycle

distributions similar to untreated cells. In contrast, treatment with 1-Ga, 1-Mn, and 1-Al resulted in stalling at the late mitotic (M) phase. Similar profiles of cell cycle distributions also were observed in breast and ovarian cancer cells incubated with these metalloporphyrins (see the Supporting Information).

Compound 1-Al appeared to induce the strongest mitotic arrest at a 30 μM dose, while varying degrees of late M arrest were also observed for Mn(III)- and Ga(III)-substituted bis-sulfonated corroles with structure 1. This late mitotic arrest, distinct from what was observed for paclitaxel (G2 arrest), suggested a mechanism other than the well-known tubulin stabilization associated with taxol derivatives. Metalloporphyrin-induced late M arrest is consistent with inhibition of cytokinesis, an event that would ultimately lead to cellular apoptosis.

Metalloporphyrins as Potential Adjuvants in Chemotherapy. The localization of 1-Ga to the nucleus of DU-145 prostate cancer cells, as well as its ability to form noncovalent complexes with a variety of molecules due to its amphiphilic nature, suggested a potential application as a carrier molecule for DNA targeting chemotherapeutic agents. The ability of 1-Ga to enhance drug cytotoxicity in DU-145 cells was examined with the DNA-intercalating anthracycline drug doxorubicin (Figure 7). IC₅₀ values were measured for doxorubicin against prostate, ovarian, and skin cancer lines in the presence of 3 μM 1-Ga. No enhancement was found for ovarian and skin cancer cells, which only showed cytoplasmic accumulation of 1-Ga; however, an ~3-fold decrease in IC₅₀ was observed for prostate carcinoma cells. In contrast, the IC₅₀ for the nonaromatic topoisomerase inhibitor etoposide in prostate cancer cells was unaffected by coadministration of 1-Ga (data not shown). The putative association of metalloporphyrins and doxorubicin is plausible in light of recent studies showing sequestration of doxorubicin by porphyrin-modified micelles.³³

CONCLUSIONS

Metalloporphyrins exhibited variable cytostatic and cytotoxic action against several human cancer cell lines. Metal ion substitution within a specific corrole nucleus influenced the biological activity. For example, substitution of Al(III) for Ga(III) significantly improved the cytotoxicity of bis-sulfonated

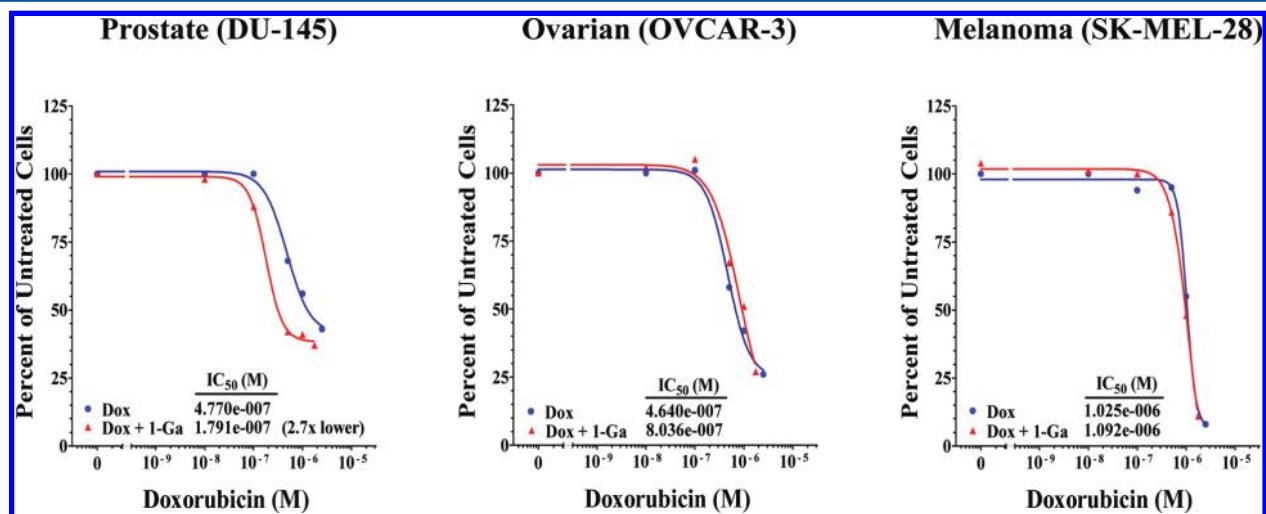


Figure 7. Effect of coadministration of 1-Ga on doxorubicin IC₅₀ values in DU-145 (prostate), OVCAR-3 (ovarian), and SK-MEL-28 (melanoma) cells. Dose–response curves from treatment with doxorubicin alone (blue) or doxorubicin + 3 μM 1-Ga (red) for 48 h.

corrole **1** and also increased the rate of cellular uptake in three unrelated cancer cell lines. However, additional structure–function studies will be required to further elucidate the influence of metal ion and functional group substitution on the biological activity of metallocorroles. Ga(III)-substituted corroles with structure **1** demonstrated dose-dependent cytostatic activity against breast, skin, and ovarian cancer cell lines. Although **1**-Ga did not exert strong cytotoxic effects in these cell lines under our assay conditions, the effective cytotoxic dose ($\sim 30 \mu\text{M}$) was comparable to other Ga(III) chelates that have been proposed as therapeutic agents^{27,28} and was much improved over Ga(III) salts that have already been tested in phase I/II clinical trials.^{24–26} Compound **1**-Ga was most active as a cytostatic agent against the SK-MEL-28 melanoma, MDA-MB-231 breast cancer, and OVCAR-3 ovarian carcinoma lines and inhibited replication of ~ 40 – 50% of the cell population at a dose of $30 \mu\text{M}$ (Figure 2B). Compound **2**-Mn displayed dose-dependent cytotoxic and cytostatic effects, with the best activity observed against the OVCAR-3 ovarian carcinoma cell line. In this case, $\sim 60\%$ of OVCAR-3 cells were killed at $30 \mu\text{M}$ **2**-Mn (Figure 3F). These effective cytotoxic doses are relatively high, but they are close to the $34 \mu\text{M}$ IC_{50} value reported for a 96 h of treatment of MDA-MB-231 breast cancer cells with cisplatin.³⁴

It has been previously demonstrated that many cytostatic agents that cause cell cycle arrest ultimately induce apoptosis or cell death.³⁵ Whether cytotoxicity follows cytostasis is largely a function of the cellular environment and depends upon the relative contributions of the different cell death mechanisms induced in response to drug treatment. Further studies with metallocorroles are required to determine whether the observed cytostasis and cell cycle arrest ultimately results in cytotoxicity. This will likely require in vivo testing using mouse xenograft models and ultimately clinical trials. Many kinase inhibitors, such as sorafenib, that were originally described as cytostatic agents prolonging progression free survival were later demonstrated in some clinical studies to ultimately induce tumor regression.³⁶

Metallocorroles used in conjunction with other drugs may also provide new approaches in cancer chemotherapy. A 3-fold improvement in the IC_{50} of doxorubicin (to $0.8 \mu\text{M}$) against a prostate cancer cell line was achieved upon coadministration with **1**-Ga (Figure 7). It is interesting to note in this regard that Ga(III) salts have been previously used in conjunction with vinblastine and ifosfamide (VIG therapy) for the treatment of cisplatin resistant urothelial cancers.³⁷ Future development of metallocorroles into useful chemotherapeutic agents would involve optimization of functional group substitution, expanded screening to uncover additional susceptible cancer cell lines, and improved intracellular targeting efficacy via covalent or noncovalent association with carrier molecules and/or proteins.

■ ASSOCIATED CONTENT

● Supporting Information

Profile of cell cycle distributions for breast and ovarian cancer cells obtained following treatment with various metallocorroles. This material is available free of charge via the Internet at <http://pubs.acs.org>.

■ AUTHOR INFORMATION

Corresponding Author

*Tel: 626-301-8169. Fax: 626-930-5463. E-mail: chr10zg@tx.technion.ac.il (Z.G.), hbgray@caltech.edu (H.B.G.), or jtermini@coh.org (J.T.).

Funding

This work was supported by Caltech-City of Hope Biomedical Research Initiative and the U.S. Army RDECOM Acquisition Center, Natick Contracting Division, Natick, MA, under Contract no. W911QY-10-C-0176.

■ ACKNOWLEDGMENTS

The technical assistance of Dr. Richard Yip and Charlie Hsin of the High Throughput Screening and Dr. Brian Armstrong of the Light Microscopy Digital Imaging Core Facilities of the City of Hope Comprehensive Cancer Center is gratefully acknowledged.

■ REFERENCES

- (1) American Cancer Society (2010) *Cancer Facts & Figures 2010*, American Cancer Society, Atlanta.
- (2) Jemal, A., Siegel, R., Xu, J., and Ward, E. (2010) Cancer statistics, 2010. *CA: Cancer J. Clin.* 60, 277.
- (3) Aviv-Harel, I., and Gross, Z. (2011) Coordination chemistry of corroles; with focus on main group elements. *Coord. Chem. Rev.* 255, 717–736.
- (4) Aviv-Harel, I., and Gross, Z. (2009) Aura of corroles. *Chem. Eur. J.* 15, 8382–8394.
- (5) Mahammed, A., Goldberg, I., and Gross, Z. (2001) Highly selective chlorosulfonation of tris(pentafluorophenyl)corrole as a synthetic tool for the preparation of amphiphilic corroles and metal complexes of planar chirality. *Org. Lett.* 3, 3443–3446.
- (6) Mahammed, A., and Gross, Z. (2005) Albumin-conjugated corrole metal complexes: Extremely simple yet very efficient biomimetic oxidation systems. *J. Am. Chem. Soc.* 127, 2883–2887.
- (7) Gershman, Z., Goldberg, I., and Gross, Z. (2007) DNA binding and catalytic properties of positively charged corroles. *Angew. Chem. Int. Ed.* 46, 4320–4324.
- (8) Ma, H., Zhang, M., Zhang, D., Huang, R., Zhao, Y., Yang, H., Liu, Y., Weng, X., Zhou, Y., Deng, M., Xu, L., and Zhou, X. (2010) Pyridyl-substituted corrole isomers: Synthesis and their regulation to G-quadruplex structures. *Chem.—Asian J.* 5, 114–122.
- (9) Saltsman, I., Botoshansky, M., and Gross, Z. (2008) Facile synthesis of ortho-pyridyl-substituted corroles and molecular structures of analogous porphyrins. *Tetrahedron Lett.* 49, 4163–4166.
- (10) Mahammed, A., Gray, H. B., Weaver, J. J., Sorasaene, K., and Gross, Z. (2004) Amphiphilic corroles bind tightly to human serum albumin. *Bioconjugate Chem.* 15, 738–746.
- (11) Haber, A., Mahammed, A., Fuhrman, B., Volkova, N., Coleman, R., Hayek, T., Aviram, M., and Gross, Z. (2008) Amphiphilic/Bipolar metallocorroles that catalyze the decomposition of reactive oxygen and nitrogen species, rescue lipoproteins from oxidative damage, and attenuate atherosclerosis in mice. *Angew. Chem. Int. Ed.* 47, 7896–7900.
- (12) Haber, A., Agadjanian, H., Medina-Kauwe, L. K., and Gross, Z. (2008) Corroles that bind with high affinity to both apo and holo transferrin. *J. Inorg. Biochem.* 102, 446–457.
- (13) Agadjanian, H., Weaver, J. J., Mahammed, A., Rentsendorj, A., Bass, S., Kim, J., Dmochowski, I. J., Margalit, R., Gray, H. B., Gross, Z., and Medina-Kauwe, L. K. (2006) Specific delivery of corroles to cells via noncovalent conjugates with viral proteins. *Pharm. Res.* 23, 367–377.
- (14) Agadjanian, H., Ma, J., Rentsendorj, A., Valluripalli, V., Hwang, J. Y., Mahammed, A., Farkas, D. L., Gray, H. B., Gross, Z., and Medina-Kauwe, L. K. (2009) Tumor detection and elimination by a targeted gallium corrole. *Proc. Natl. Acad. Sci. U.S.A.* 106, 6105–6110.

- (15) Aviezer, D., Cotton, S., David, M., Segev, A., Khaselev, N., Galili, N., Gross, Z., and Yayon, A. (2000) Porphyrin analogues as novel antagonists of fibroblast growth factor and vascular endothelial growth factor receptor binding that inhibit endothelial cell proliferation, tumor progression, and metastasis. *Cancer Res.* 60, 2973–2980.
- (16) Berg, K., Selbo, P. K., Weyergang, A., Dietze, A., Prasmickaite, L., Bonsted, A., Engesaeter, B. O., Angell-Petersen, E., Warloe, T., Frandsen, N., and Hogset, A. (2005) Porphyrin-related photosensitizers for cancer imaging and therapeutic applications. *J. Microsc.* 218, 133–147.
- (17) Shoemaker, R. H. (2006) The NCI60 human tumour cell line anticancer drug screen. *Nature Rev.* 6, 813–823.
- (18) Saltsman, I., Mahammed, A., Goldberg, I., Tkachenko, E., Botoshansky, M., and Gross, Z. (2002) Selective substitution of corroles: Nitration, hydroformylation, and chlorosulfonation. *J. Am. Chem. Soc.* 124, 7411–7420.
- (19) Haber, A., Aviram, M., and Gross, Z. (2011) Protecting the beneficial functionality of lipoproteins by 1-Fe, a corrole-based catalytic antioxidant. *Chem. Sci.* 2, 295–302.
- (20) Richardson, D. R. (2001) Iron and gallium increase iron uptake from transferrin by human melanoma cells: Further examination of the ferric ammonium citrate-activated iron uptake process. *Biochim. Biophys. Acta* 1536, 43–54.
- (21) Tampo, Y., Kotamraju, S., Chitambar, C. R., Kalivendi, S. V., Keszler, A., Joseph, J., and Kalyanaraman, B. (2003) Oxidative stress-induced iron signaling is responsible for peroxide-dependent oxidation of dichlorodihydrofluorescein in endothelial cells: Role of transferrin receptor-dependent iron uptake in apoptosis. *Circ. Res.* 92, 56–63.
- (22) Chitambar, C. R., Narasimhan, J., Guy, J., Sem, D. S., and O'Brien, W. J. (1991) Inhibition of ribonucleotide reductase by gallium in murine leukemic L1210 cells. *Cancer Res.* 51, 6199–6201.
- (23) Jakupec, M. A., and Keppler, B. K. (2004) Gallium in cancer treatment. *Curr. Top. Med. Chem.* 4, 1575–1583.
- (24) Chitambar, C. R. (2010) Medical applications and toxicities of gallium compounds. *Int. J. Environ. Res. Public Health* 7, 2337–2361.
- (25) Hedley, D. W., Tripp, E. H., Slowiaczek, P., and Mann, G. J. (1988) Effect of gallium on DNA synthesis by human T-cell lymphoblasts. *Cancer Res.* 48, 3014–3018.
- (26) Seidman, A. D., Scher, H. I., Heinemann, M. H., Bajorin, D. F., Sternberg, C. N., Dershaw, D. D., Silverberg, M., and Bosl, G. J. (1991) Continuous infusion gallium nitrate for patients with advanced refractory urothelial tract tumors. *Cancer* 68, 2561–2565.
- (27) Chitambar, C. R., Purpi, D. P., Woodliff, J., Yang, M., and Wereley, J. P. (2007) Development of gallium compounds for treatment of lymphoma: gallium maltolate, a novel hydroxypyron gallium compound, induces apoptosis and circumvents lymphoma cell resistance to gallium nitrate. *J. Pharmacol. Exp. Ther.* 322, 1228–1236.
- (28) Chua, M. S., Bernstein, L. R., Li, R., and So, S. K. (2006) Gallium maltolate is a promising chemotherapeutic agent for the treatment of hepatocellular carcinoma. *Anticancer Res.* 26, 1739–1743.
- (29) Candide, C., Morliere, P., Maziere, J. C., Goldstein, S., Santus, R., Dubertret, L., Reyftmann, J. P., and Polonovski, J. (1986) In vitro interaction of the photoactive anticancer porphyrin derivative photofrin II with low density lipoprotein, and its delivery to cultured human fibroblasts. *FEBS Lett.* 207, 133–138.
- (30) Maziere, J. C., Morliere, P., and Santus, R. (1991) The role of the low density lipoprotein receptor pathway in the delivery of lipophilic photosensitizers in the photodynamic therapy of tumours. *J. Photochem. Photobiol. B* 8, 351–360.
- (31) Krishnamurthy, P. C., Du, G., Fukuda, Y., Sun, D., Sampath, J., Mercer, K. E., Wang, J., Sosa-Pineda, B., Murti, K. G., and Schuetz, J. D. (2006) Identification of a mammalian mitochondrial porphyrin transporter. *Nature* 443, 586–589.
- (32) Richardson, D., and Baker, E. (1992) Two mechanisms of iron uptake from transferrin by melanoma cells. The effect of desferrioxamine and ferric ammonium citrate. *J. Biol. Chem.* 267, 13972–13979.
- (33) Lovell, J. F., Jin, C. S., Huynh, E., Jin, H., Kim, C., Rubinstein, J. L., Chan, W. C., Cao, W., Wang, L. V., and Zheng, G. (2011) Porphysome nanovesicles generated by porphyrin bilayers for use as multimodal biophotonic contrast agents. *Nat. Mater.* 10, 324–332.
- (34) Pope, A. J., Bruce, C., Kysela, B., and Hannon, M. J. (2010) Issues surrounding standard cytotoxicity testing for assessing activity of non-covalent DNA-binding metallo-drugs. *Dalton Trans.* 39, 2772–2774.
- (35) Zaffaroni, N., Silvestrini, R., Orlandi, L., Bearzatto, A., Gornati, D., and Villa, R. (1998) Induction of apoptosis by taxol and cisplatin and effect on cell cycle-related proteins in cisplatin-sensitive and -resistant human ovarian cells. *Br. J. Cancer* 77, 1378–1385.
- (36) Escudier, B., Eisen, T., Stadler, W. M., Szczylik, C., Oudard, S., Siebels, M., Negrier, S., Chevreau, C., Solska, E., Desai, A. A., Rolland, F., Demkow, T., Hutson, T. E., Gore, M., Freeman, S., Schwartz, B., Shan, M., Simantov, R., and Bukowski, R. M. (2007) Sorafenib in advanced clear-cell renal-cell carcinoma. *N. Engl. J. Med.* 356, 125–134.
- (37) Einhorn, L. H., Roth, B. J., Ansari, R., Dreicer, R., Gonin, R., and Loehrer, P. J. (1994) Phase II trial of vinblastine, ifosfamide, and gallium combination chemotherapy in metastatic urothelial carcinoma. *J. Clin. Oncol.* 12, 2271–2276.